

Maximum droplet volume on cylindrical surfaces

Yi Zhang¹, Apurav Tambe¹, and Zhao Pan^{*1}

¹University of Waterloo, Department of Mechanical and Mechatronics Engineering,
Waterloo, ON, Canada

December 29, 2025

Abstract

The maximum volume (Ω) of a droplet that can remain attached to a horizontal fiber defines the stability limit of droplet-fiber interactions, phenomena common in nature and critical to diverse engineering applications. Existing predictive models for Ω show limitations in accurately capturing the dependence of Ω on fiber size and wettability. To address this gap, we systematically investigate Ω on a horizontal fiber through numerical simulations and experiments. A comprehensive semi-empirical model for Ω is developed and validated against both experimental measurements and reference simulations. This model establishes a new scaling under which the normalized maximum droplet volume depends solely on the contact angle and remains valid across a wide spectrum from a sub-millimeter thin fiber to the flat-surface limit, regardless of the diverse morphologies that droplets exhibit.

Key words: Droplet; Horizontal fiber; Maximum volume; Capillary length; Contact angle

1 Introduction

The largest droplet that can hang from a ceiling before it falls under gravity is a classic manifestation of the Rayleigh-Taylor instability [1], and has remained an enduring subject of investigation [2–4].

*To whom correspondence may be addressed: zhao.pan@uwaterloo.ca

Established results reveal that the dimensionless maximum volume of such a droplet ($\bar{\Omega}_* = \bar{\Omega}/\lambda^3$, where $\bar{\Omega}$ is the dimensional maximum volume and λ is liquid capillary length) depends solely on the surface contact angle (θ) [2]. Imagine “rolling up” the ceiling into a cylinder: the problem of a droplet hanging beneath a plane naturally transforms into that of a droplet hanging on a fiber (despite the markedly altered droplet morphology), a system that has also been extensively studied [5–7].

Droplet-fiber interactions are pervasive in both nature and engineering applications, from spider webs capturing water to engineered fibers designed for separation and harvesting devices [8–11]. Among the many phenomena in this setting, a fundamental question is again the maximum droplet volume (Ω) that a horizontal fiber can sustain, which has critical implications for applications such as fog harvesting [11–14], as well as filtration and separation [15, 16].

To address this deceptively simple question, Lorenceau et al. [17] developed a widely adopted analytical model for droplets on thin fibers (fiber radius $r \ll \lambda$), given by

$$\Omega_* = \frac{\Omega}{\lambda^2 r} = 4\pi, \quad (1)$$

where Ω_* denotes the dimensionless maximum droplet volume on a fiber. To account for θ , Wang and Olivier [18] modified the model to $\Omega = 4\pi r \lambda^2 \cos \theta$. Moreover, Pan et al. [19] employed a free-energy analysis and derived $\Omega = 4\pi r \lambda^2 \sin \beta$, where β is the droplet off-axis angle influenced by θ . However, determining β requires experimental input. These models share the same underlying assumption: the three-phase contact line (TCL) is approximated by two complete circumferences of the fiber cross-section, giving a TCL length of $4\pi r$. However, as the droplet volume approaches its maximum, it becomes energetically favorable for the droplet to adopt a clam-shell morphology [20, 21], in which the droplet no longer fully wraps the fiber, and the TCL is not circular but instead becomes irregular. This breakdown is pronounced on thick fibers or at low liquid-solid wettability [21], leading to marked discrepancies between theoretical predictions [17, 18] and collected data (see Electronic Support Information (ESI) Section 1). Furthermore, as the fiber thickens and approaches a flat-surface geometry, Ω should asymptotically converge to the planar ceiling limit $\bar{\Omega}_* \lambda^3$. Yet, no existing framework has been able to quantitatively capture this transition.

In this letter, we develop a comprehensive model that spans a wide spectrum from thin fibers to the flat-surface limit, while explicitly incorporating the role of θ . It resolves the long-standing problem of how droplet retention evolves with fiber radius, bridging the classic “droplet-on-ceiling” problem with its cylindrical analogue, “droplet-on-fiber”.

2 Methods

2.1 Simulation by surface evolver

Surface Evolver (SE, version 2.70) [22] is employed to investigate the maximum droplet volume (Ω) on a horizontal fiber by simulating the profiles of droplets of progressively increasing volume until detachment occurs. In SE, the liquid phase is initialized as a cuboid-shaped slab positioned beneath a cylindrical fiber with radius (r) and prescribed liquid-solid contact angle (θ), see the simulation setup in ESI Section 2. The liquid is characterized by its surface tension (γ), density (ρ), and volume (V). SE evolves the liquid cuboid towards its equilibrium shape by minimizing the total free energy (F), given by [21]

$$F = \gamma(A_{LV} - A_{LS} \cos \theta) + \iiint \rho g z dV, \quad (2)$$

where A_{LV} and A_{LS} are the liquid-vapor and liquid-solid interfacial area, respectively, and the last term represents the gravitational potential energy. The simulation starts with a small V for which the droplet remains stably attached to the fiber ($V \leq \Omega$). The volume is then increased stepwise by 0.5 μL until detachment occurs ($V > \Omega$), marking the maximum supported volume (see Figure S2).

In this work, simulations are conducted for θ ranging from 1° to 90° and r from 0.1 mm to 9 mm. The liquid capillary length, defined as $\lambda = \sqrt{\gamma/(\rho g)}$, is varied from 1.4 mm to 2.7 mm. This variation is achieved by adjusting γ in the range of 20 mN/m to 70 mN/m, and ρ from $0.7 \times 10^3 \text{ kg/m}^3$ to $1.00 \times 10^3 \text{ kg/m}^3$. The parameters θ , r , and λ are sampled at a discrete set of representative values, and all combinations within these sets are systematically simulated for Ω .

2.2 Experimental validation

The maximum droplet volumes for various liquid-fiber pairs are measured experimentally. The test liquid is gradually dispensed onto a horizontally mounted fiber using an electronic pipette until detachment, and the dispensed volume is recorded as Ω . Table S1 summarizes the tested liquid-fiber pairs and their physical properties. Six liquids with γ ranging from 21 mN/m to 72 mN/m and λ from 1.5 mm to 2.7 mm are employed. Fibers of five different materials covering θ from 0° to 70° are examined, with r varied between 0.1 mm and 19.1 mm. Details of the experimental setup and procedures are provided in ESI Section 3. Additionally, experimental and simulation data from the literature [19, 21, 23] are incorporated for external validation.

3 Results and discussion

3.1 Simulation results and semi-empirical model development

Figure 1(A) presents the SE simulated values of Ω_* as a function of the normalized fiber radius ($r_* = r/\lambda$) for various contact angles (θ). In contrast to the constant prediction by Eq (1), Ω_* decreases with increasing θ and r_* . By rescaling the simulation results onto a logarithmic scale (inset), we observe that the slope of $\Omega_*(r_*, \theta)$ on the log-log plot mostly varies with r_* . This indicates a potential power-law relationship between Ω_* and r_* , characterized by a variable exponent n that captures the slope variation. Accordingly, we propose the following relationship:

$$\Omega_* = \frac{\Omega}{\lambda^2 r} \approx \bar{\Omega}_* r_*^{-n}, \quad (3)$$

where $\bar{\Omega}_*$ denotes the normalized maximum droplet volume under a flat surface. Although there is no known closed solution for $\bar{\Omega}_*$, numerical results such as the seminal envelope curve (adopted here) developed by Padday and Pitt [2], and several subsequent empirical models [3, 4, 24] are available. We construct the exponent n taking the form

$$n = \frac{a}{r_* - 1} + 1, \quad (4)$$

The parameter, a , is determined by fitting eq (3) to the data in Figure 1(A). The fitted values of a are presented in Figure 1(B) as a function of $\cos \theta$, revealing a linear dependence given by

$$a \approx 0.32 \cos \theta + 0.64. \quad (5)$$

Eq (3) can thus be expressed as

$$\Omega_* = \frac{\Omega}{\lambda^2 r} \approx \bar{\Omega}_* r_*^{-\left(\frac{0.32 \cos \theta + 0.64}{r_* - 1} + 1\right)}. \quad (6)$$

In the limiting cases, the asymptotic behaviors of eq (6) are consistent with physical expectations. As $r_* \rightarrow \infty$ (i.e., when the fiber becomes sufficiently thick to approximate a flat surface), it reduces to $\Omega/\lambda^3 \approx \bar{\Omega}_*$, recovering the classic “droplet-on-ceiling” limit. As $r_* \rightarrow 0$, eq (6) yields $\Omega \rightarrow 0$, as no solid surface exists to support the droplet. For finite but small r_* ($r_* \ll 1$), eq (6) simplifies to $\Omega/\lambda^{2.04} r^{0.96} \approx \bar{\Omega}_*$ under high wettability, closely resembles the scaling by Lorenceau et al., as relisted in eq (1) [17]. This formulation illustrates the evolution of the maximum droplet volume as r increases from a thin fiber to a flat surface, and explicitly incorporates the role of θ .

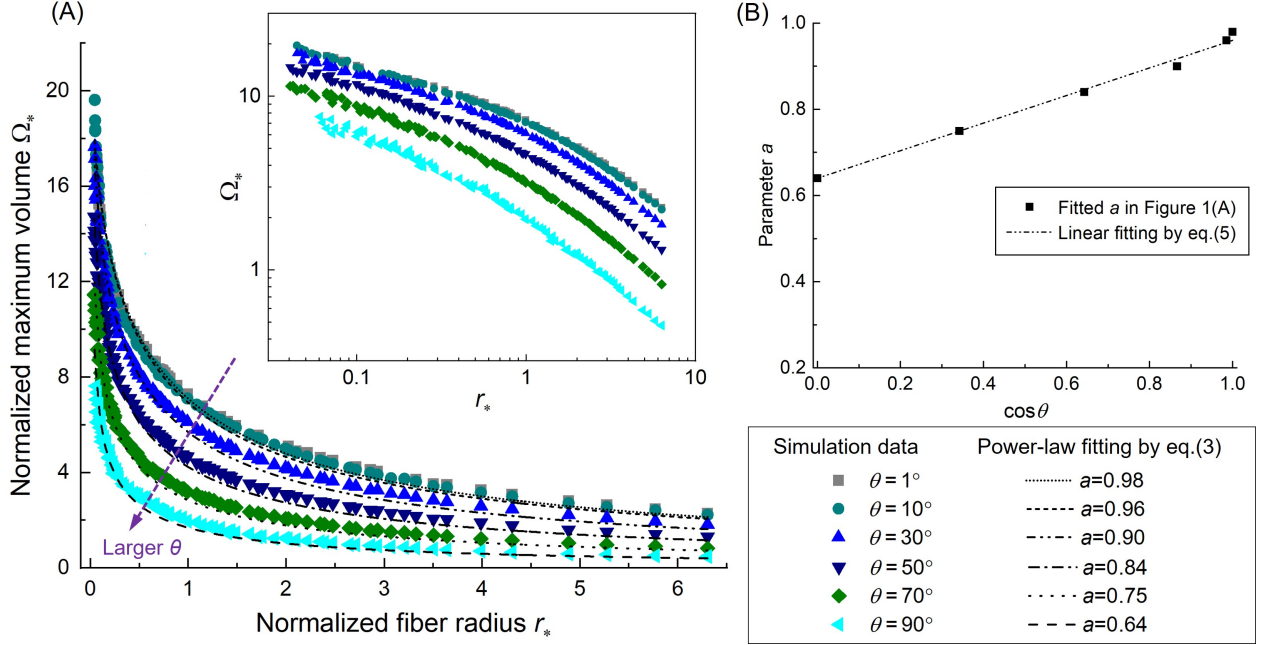


Figure 1: (A) Simulation results of the normalized maximum droplet volume ($\Omega_* = \Omega/\lambda^2 r$) as a function of the normalized fiber radius ($r_* = r/\lambda$) for various contact angles (θ). Power-law fits of Ω_* follow eq (3). (B) Fitted values of parameter a corresponding to (A).

Another way to interpret eq (6) is to rearrange the r_* -dependent factor to the left-hand side of the equation, leading to a new normalization of Ω , denoted as Ω_\dagger :

$$\Omega_\dagger = \frac{\Omega}{\lambda^3} r_*^{n-1} = C(r_*, \theta) \frac{\Omega}{\lambda^3} \approx \bar{\Omega}_*(\theta), \quad (7)$$

where $C(r_*, \theta) = r_*^{\frac{0.32 \cos \theta + 0.64}{r_* - 1}}$ is a dimensionless coefficient. Remarkably, $C(r_*, \theta)$ enables a new scaling that eliminates the contribution from the cylinder diameter r_* , and the normalized maximum droplet volume on a fiber can be approximated by the flat-surface value $\bar{\Omega}_*$, depending solely on θ .

3.2 Validation and discussion

Figure 2(A) validates the comprehensive model given by eq (7) for predicting the maximum droplet volume on a horizontal fiber. Validation is performed against simulation results from an earlier work [21] as well as experimental data obtained both in our laboratory and from the literature [19, 23]. Across these datasets, r_* spans a wide range from 0.04 to 12.55, with the upper limit close to a flat surface. As an illustration, at $r_* = 12.55$, the dimensionless coefficient C in eq (7) reaches ~ 1.23 under perfect wetting, implying that Ω on such a fiber exceeds 80% (or $1/1.23$) of

that under a flat surface. All Ω are normalized to Ω_{\dagger} following eq (7). As shown in Figure 2(A), Ω_{\dagger} for different r_* and θ collapse onto a single curve $\bar{\Omega}_*(\theta)$, in contrast to the broad variation of Ω_* observed in Figures 1 and S1, thereby validating the relation $C(r_*, \theta) \frac{\Omega}{\lambda^3} \approx \bar{\Omega}_*(\theta)$ of eq (7). This collapse is independent of the various droplet morphologies across varying r_* and θ (see discussion below). The inset of Figure 2(A) plots Ω_{\dagger} versus $\bar{\Omega}_*(\theta)$. All data fall reasonably well on the $\Omega_{\dagger} = \bar{\Omega}_*$ line (dashed), confirming $\Omega_{\dagger} \approx \bar{\Omega}_*(\theta)$ of eq (7). Overall, the model agrees well with both the experimental data and the reference simulations, with a mean relative error of 10.0%.

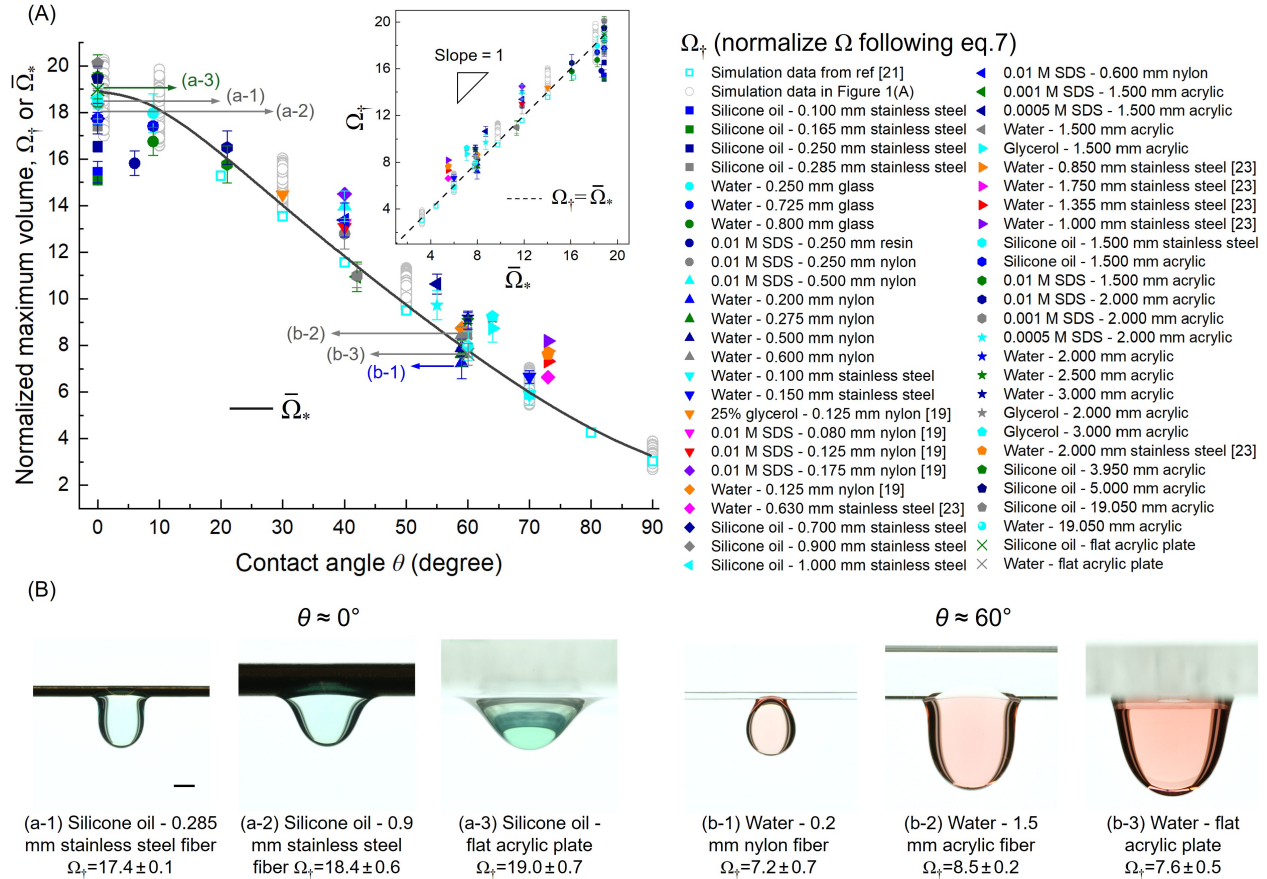


Figure 2: (A) Validation of the developed semi-empirical model, given by eq (7), for predicting the maximum droplet volume on a horizontal fiber. The legend on the right specifies the liquid type, fiber radius, and fiber material. Error bars represent the standard deviation from three to five repeated measurements. (B) Photos of maximum-volume droplets suspended beneath fibers and flat surfaces for $\theta \approx 0^\circ$ and $\theta \approx 60^\circ$, corresponding to the marked data points in (A). Scale bar indicates 0.5 mm.

Figure 2(B) exemplifies the morphologies of maximum-volume droplets suspended beneath var-

ious fibers and flat surfaces for $\theta \approx 0^\circ$ and $\theta \approx 60^\circ$. For a given θ , droplets adopt distinct shapes as r_* varies. The mechanisms governing droplet instability also differ: de-pinning of TCL for thin fibers while necking of droplets for flat surfaces, as discussed in our previous work [24]. Despite these contrasting behaviors, the proposed model provides a unified scaling. With the scaling coefficient $C(r_*, \theta)$, Ω_\dagger for cylindrical fibers, even across different r_* , collapses onto $\bar{\Omega}_*$ for flat surfaces at a given θ , thereby recovering the classic “droplet-on-ceiling” limit.

The physics underlying eq (7) may be understood from the asymmetric contact line of a droplet on a fiber. We characterize the droplet’s degree of symmetry by the ratio (W/L) between the wetting width W across the fiber and the wetting length L along the fiber (see Figure 3). For small r_* , the droplet exhibits a low degree of symmetry (small W/L), and its maximum volume (Ω) deviates markedly from the flat-surface value ($\bar{\Omega}$). Increasing r_* enhances the symmetry (larger W/L), and Ω progressively approaches $\bar{\Omega}$. In the flat-surface limit, symmetry is restored with $W/L = 1$ and $\Omega/\bar{\Omega} = 1$. Our simulations reveal (see Figure 3(A)) a simple scaling relation $\Omega/\bar{\Omega} \approx (W/L)^b$, where $b = 1.00, 1.27,$ and 1.43 for $\theta = 10^\circ, 50^\circ,$ and 90° , respectively. These values are well captured by the fit $b = 0.5 \sin \theta + 0.9$.

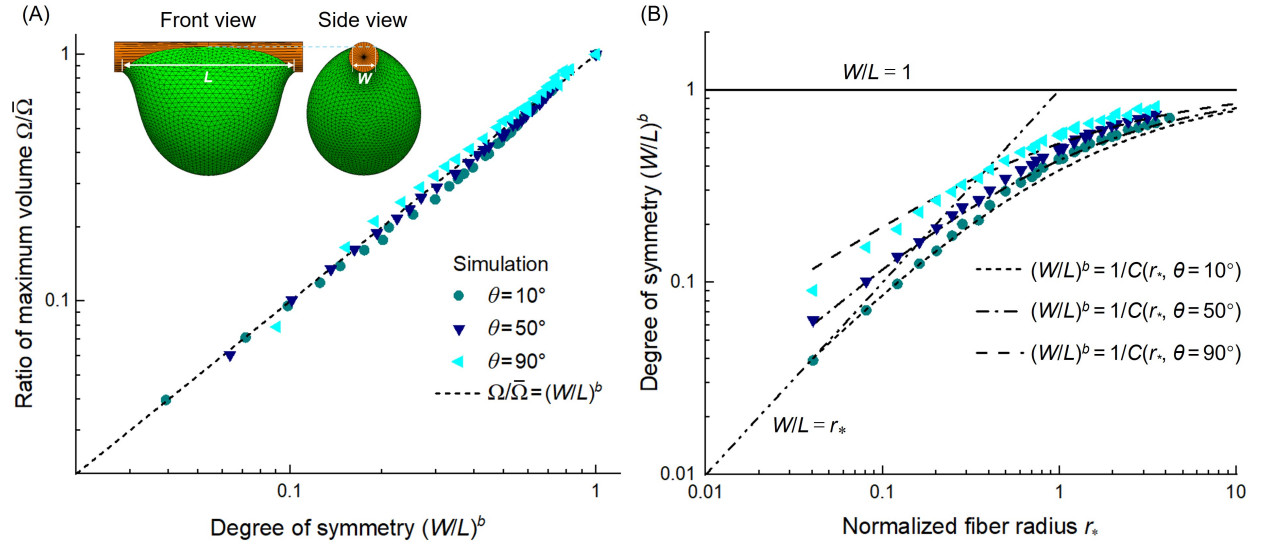


Figure 3: Degree of droplet symmetry, characterized by the ratio of the wetting width W across the fiber to the wetting length L along the fiber. (A) $\Omega/\bar{\Omega}$, the ratio between the maximum droplet volume on a fiber (Ω) and that beneath a flat surface ($\bar{\Omega}$) under the same λ and θ , as a function of $(W/L)^b$, where $b = 0.5 \sin \theta + 0.9$. (B) $(W/L)^b$ as a function of r_* . Point symbols correspond to those in (A).

Figure 3(B) further illustrates how $(W/L)^b$ depends on r_* . Under well-wetting conditions (e.g., $\theta = 10^\circ$), for small r_* the lateral (W) and axial (L) wetting are dominated by r and λ , respectively, leading to the asymptotic behavior $W/L \rightarrow r_*$ as $r_* \rightarrow 0$ (dash-dot-dot line). In the opposite limit ($r_* \rightarrow \infty$), the geometry approaches a flat surface and $W/L \rightarrow 1$ (solid line). As an example, the relation $(W/L)^b = 1/C(r_*, \theta = 10^\circ)$ (short-dashed line) bridges these two limits and shows reasonable agreement with the simulations. Inserting this relation into the scaling $\Omega/\bar{\Omega} \approx (W/L)^b$ in Figure 3(A) recovers eq. (7), i.e., $\Omega/\bar{\Omega} \approx 1/C(r_*, \theta)$. For large θ , the asymptotic scaling $W/L \rightarrow r_*$ as $r_* \rightarrow 0$ no longer holds, as θ significantly suppresses droplet spreading along the fiber L . Nevertheless, the expressions $(W/L)^b = 1/C(r_*, \theta = 50^\circ)$ and $(W/L)^b = 1/C(r_*, \theta = 90^\circ)$ remain in reasonable agreement with the simulations for $\theta = 50^\circ$ and $\theta = 90^\circ$, respectively.

4 Conclusion

In summary, this work systematically investigates the ability of horizontal fibers to retain liquid droplets. We develop and validate a unified semi-empirical model for the maximum droplet volume (Ω), expressed as $C \frac{\Omega}{\lambda^3} \approx \bar{\Omega}_*$, where C is a dimensionless coefficient dependent on the normalized fiber radius and contact angle; λ is the capillary length; $\bar{\Omega}_*$ is the normalized maximum droplet volume under the corresponding flat surface. The model remains valid across the wide transition from a sub-millimeter thin fiber to the flat-surface limit. We further show that Ω is governed by the degree of symmetry of the droplet, as it becomes asymmetric when wetting a cylindrical fiber.

Acknowledgement

The authors gratefully acknowledge the financial support provided by the Artificial Intelligence for Design Challenge (AI4D) program, funded by the National Research Council Canada.

References

- [1] Geoffrey Ingram Taylor. The instability of liquid surfaces when accelerated in a direction perpendicular to their planes. i. *Proceedings of the Royal Society of London. Series A. Mathematical and Physical Sciences*, 201(1065):192–196, 1950.
- [2] JF Padday and AR Pitt. The stability of axisymmetric menisci. *Philosophical Transactions of*

- the Royal Society of London. Series A, Mathematical and Physical Sciences*, 275(1253):489–528, 1973.
- [3] Dan Daniel and Xue Qi Koh. Droplet detachment force and its relation to young–dupre adhesion. *Soft matter*, 19(43):8434–8439, 2023.
- [4] Muhammad Subkhi Sadullah, Yinfeng Xu, Sankara Arunachalam, and Himanshu Mishra. Predicting droplet detachment force: Young–dupré model fails, young–laplace model prevails. *Communications Physics*, 7(1):89, 2024.
- [5] Brendan Joseph Carroll. The equilibrium of liquid drops on smooth and rough circular cylinders. *Journal of Colloid and Interface Science*, 97(1):195–200, 1984.
- [6] BJ Carroll. Equilibrium conformations of liquid drops on thin cylinders under forces of capillarity. a theory for the roll-up process. *Langmuir*, 2(2):248–250, 1986.
- [7] John F Bitten. Coalescence of water droplets on single fibers. *Journal of colloid and interface science*, 33(2):265–271, 1970.
- [8] Yongmei Zheng, Hao Bai, Zhongbing Huang, Xuelin Tian, Fu-Qiang Nie, Yong Zhao, Jin Zhai, and Lei Jiang. Directional water collection on wetted spider silk. *Nature*, 463(7281):640–643, 2010.
- [9] C Duprat, S Protiere, AY Beebe, and Howard A Stone. Wetting of flexible fibre arrays. *Nature*, 482(7386):510–513, 2012.
- [10] Jie Ju, Hao Bai, Yongmei Zheng, Tianyi Zhao, Ruochen Fang, and Lei Jiang. A multi-structural and multi-functional integrated fog collection system in cactus. *Nature communications*, 3(1):1247, 2012.
- [11] Kyoo-Chul Park, Shreerang S Chhatre, Siddarth Srinivasan, Robert E Cohen, and Gareth H McKinley. Optimal design of permeable fiber network structures for fog harvesting. *Langmuir*, 29(43):13269–13277, 2013.
- [12] Qiuting Zhang, Gaojian Lin, and Jie Yin. Highly efficient fog harvesting on superhydrophobic microfibers through droplet oscillation and sweeping. *Soft Matter*, 14(41):8276–8283, 2018.
- [13] Yongping Hou, Yuan Chen, Yan Xue, Yongmei Zheng, and Lei Jiang. Water collection behavior and hanging ability of bioinspired fiber. *Langmuir*, 28(10):4737–4743, 2012.

- [14] Arani Mukhopadhyay, Arkadeep Datta, Partha Sarathi Dutta, Amitava Datta, and Ranjan Ganguly. Droplet morphology-based wettability tuning and design of fog harvesting mesh to minimize mesh-clogging. *Langmuir*, 40(15):8094–8107, 2024.
- [15] Wenquan Gu, Shenglin Yan, and Zhishan Bai. A study on a droplet impact on a fiber during coalescence-separation: Phenomena and models. *Chemical Engineering Science*, 212:115337, 2020.
- [16] J Fang, M Davoudi, and GG Chase. Drop movement along a fiber axis due to pressure driven air flow in a thin slit. *Separation and Purification Technology*, 140:77–83, 2015.
- [17] Élise Lorenceau, Christophe Clanet, and David Quéré. Capturing drops with a thin fiber. *Journal of colloid and interface science*, 279(1):192–197, 2004.
- [18] Sheng Wang and Olivier Desjardins. Numerical study of the critical drop size on a thin horizontal fiber: Effect of fiber shape and contact angle. *Chemical Engineering Science*, 187:127–133, 2018.
- [19] Zhao Pan, Floriane Weyer, William G Pitt, Nicolas Vandewalle, and Tadd T Truscott. Drop on a bent fibre. *Soft Matter*, 14(19):3724–3729, 2018.
- [20] Glen McHale and MI Newton. Global geometry and the equilibrium shapes of liquid drops on fibers. *Colloids and Surfaces A: Physicochemical and Engineering Aspects*, 206(1-3):79–86, 2002.
- [21] Tung-He Chou, Siang-Jie Hong, Yu-En Liang, Heng-Kwong Tsao, and Yu-Jane Sheng. Equilibrium phase diagram of drop-on-fiber: coexistent states and gravity effect. *Langmuir*, 27(7):3685–3692, 2011.
- [22] Kenneth A Brakke. The surface evolver. *Experimental mathematics*, 1(2):141–165, 1992.
- [23] Arkadeep Datta, Arani Mukhopadhyay, Partha Sarathi Dutta, Arijit Saha, Amitava Datta, and Ranjan Ganguly. Droplet detachment from a horizontal fiber of a fog harvesting mesh. In *Conference on Fluid Mechanics and Fluid Power*, pages 485–490. Springer, 2021.
- [24] Yi Zhang and Zhao Pan. Droplets suspended beneath a fiber hub. *Langmuir*, 41(23):14977–14984, 2025.